Environmental Pollution 320 (2023) 120997

Contents lists available at ScienceDirect

Environmental Pollution

journal homepage: www.elsevier.com/locate/envpol

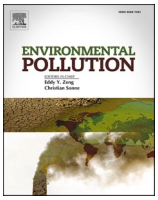

Role of vertical advection and diffusion in long-range $PM_{2.5}$ transport in Northeast Asia☆

Eunhye Kim [a], Byeong-Uk Kim [b], Yoon-Hee Kang [c], Hyun Cheol Kim [c,d], Soontae Kim [a,*]

[a] Department of Environmental & Safety Engineering, Ajou University, Suwon, 16499, South Korea
[b] Georgia Environmental Protection Division, Atlanta, GA, 30354, USA
[c] Air Resources Laboratory, National Oceanic and Atmospheric Administration, College Park, MD, 20740, USA
[d] Cooperative Institute for Satellite Earth System Studies, University of Maryland, College Park, MD, 20740, USA

ARTICLE INFO

Keywords:
Particulate matter
LRT
Vertical mixing
Downdraft
Mixing down
PBL

ABSTRACT

This study quantitatively analyzed the role of vertical mixing in long-range transport (LRT) of $PM_{2.5}$ during its high concentration episode in Northeast Asia toward the end of February 2014. The $PM_{2.5}$ transport process from an upwind to downwind area was examined using the Community Multi-scale Air Quality (CMAQ) modeling system with its instrumented tool and certain code modifications. We identified serial distinctive roles of vertical advection (ZADV) and diffusion (VDIF) processes. The surface $PM_{2.5}$ in an upwind area became aloft by VDIF—during daytime—to the planetary boundary layer (PBL) altitude of 1 km or lower. In contrast, ZADV updraft effectively transported $PM_{2.5}$ vertically to an altitude of 2–3 km above the PBL. Furthermore, we found that the VDIF and ZADV in the upwind area synergistically promoted the vertical mixing of air pollutants up to an altitude of 1 km and higher. The aloft $PM_{2.5}$ in the upwind area was then transported to the downwind area by horizontal advection (HADV), which was faster than HADV at the surface layer. Additionally, VDIF and ZADV over the downwind area mixed down the aloft $PM_{2.5}$ on the surface. During this period, the VDIF and ZADV increased the $PM_{2.5}$ concentrations in the downwind area by up to 15 $\mu g \cdot m^{-3}$ (15%) and 101 $\mu g \cdot m^{-3}$ (60%), respectively. This study highlights the importance of vertical mixing on long-range $PM_{2.5}$ transport and warrants more in-depth model analysis with three-dimensional observations to enhance its comprehensive understanding.

1. Introduction

Air pollutants emitted into the atmosphere in an upwind area are transported to downwind areas by advection and diffusion (Ge et al., 2018; Seinfeld and Pandis, 2006; Sharan et al., 1996; Shen et al., 2022). Previous studies have reported that they can travel horizontally over long distances (i.e., several hundreds to thousands of kilometers) depending on the meteorological conditions (Chen et al., 2021; Li et al., 2017a; Seo et al., 2017). Therefore, for certain regions, countries situated downwind should consider the long-range transport of air pollutants from those located upwind when they develop their own domestic air quality management planning (Chen et al., 2014; Choi et al., 2019; Reis et al., 2012; Uno et al., 2020).

The Northeast Asia region is in the westerly wind zone (Park et al., 2009; Seinfeld and Pandis, 2006). During the northwest monsoon period (i.e., October to late March), the impact of the long-range transport of air pollutants emitted from the upwind area on downwind areas becomes more intense in this region (Bae et al., 2019; Itahashi et al., 2017; Shimadera et al., 2016; Wang et al., 2016). In addition to this seasonal weather pattern, the long-range transport of air pollutants is affected by synoptic-scale weather conditions, including high/low pressure systems (Xiao et al., 2020; Lee et al., 2019a; Pei et al., 2018; Lee et al., 2011). Kim et al. (2016) analyzed the long-range transport of PM_{10} by classifying the synoptic patterns into three types in Northeast Asia. You et al. (2021) and Chuang et al. (2008) analyzed the duration of high $PM_{2.5}$ concentrations and the change in the pathway and scale of long-range transport depending on the locations of high/low pressure systems in Northeast Asia.

Recent studies have examined the role of vertical mixing during the long-range transport of air pollutants. Lei et al. (2021) and Liu et al., 2021 reported that diurnal boundary layer dynamics and regional transport affected the surface $PM_{2.5}$ concentrations. Lee et al. (2019b)

☆ This paper has been recommended for acceptance by Pavlos Kassomenos.
* Corresponding author.
E-mail address: soontaekim@ajou.ac.kr (S. Kim).

https://doi.org/10.1016/j.envpol.2022.120997
Received 11 October 2022; Received in revised form 7 December 2022; Accepted 31 December 2022
Available online 5 January 2023
0269-7491/© 2023 The Authors. Published by Elsevier Ltd. This is an open access article under the CC BY license (http://creativecommons.org/licenses/by/4.0/).

and Kim et al. (2021a) also reported that long-range air pollutants that were transported from upwind through the residual layer influenced the surface $PM_{2.5}$ concentrations in downwind areas via vertical mixing. These studies indicated that vertical mixing can be important for the long-range transport of air pollutants. However, studies on the quantitative assessment of the role of vertical mixing during regional air pollutant transport in Northeast Asia are lacking.

Vertical mixing comprises vertical advection (ZADV) and vertical diffusion (VDIF). ZADV can exert regional influence for several days to weeks because it is a dominant atmospheric process at the synoptic scale (Pei et al., 2018), while VDIF can have a more localized influence for several hours to days because it is a dominant atmospheric process at the local scale (Seaman et al., 2000; Yan et al., 2022). The net effect of vertical transport on long-range $PM_{2.5}$ transport depends on the relative intensity and spatiotemporal characteristics of ZADV and VDIF. Hence, for better understand about the mechanism of long-range $PM_{2.5}$ transport, it is necessary to analyze ZADV and VDIF separately.

In this study, we investigated the role of vertical mixing in the long-range transport of $PM_{2.5}$ using an air quality model. In our study, we selected the prolonged long-range $PM_{2.5}$ episode of Northeast Asia that occurred toward the end of February 2014 (Park et al., 2018; Shin et al., 2016; Kim et al., 2017a; and Kim et al., 2017b). First, the inflow pathways of the air pollutants at the surface and high altitudes of the downwind area during the episode were examined. Then, vertical distributions of the $PM_{2.5}$ concentrations and the effect of upwind emissions were analyzed using the estimated pathway. We also examined the contributions of ZADV and VDIF to the $PM_{2.5}$ concentrations in the upwind and downwind areas. Finally, the sensitivity of the ground level $PM_{2.5}$ concentrations in these areas to changes in the ZADV and VDIF were evaluated to quantitatively understand their roles in the long-range transport of air pollutants.

2. Methods

2.1. Study area and period

One of the most severe $PM_{2.5}$ event in the past decade over Northeast Asia occurred during late February of 2014, which has been extensively studied (Wang et al., 2018; Shin et al., 2016; Kim et al., 2017a; Kim et al., 2017b). The recorded average $PM_{2.5}$ concentrations at the surface from February 22–27, 2014, were 277.5 $\mu g \cdot m^{-3}$ in Beijing, China and 122.7 $\mu g \cdot m^{-3}$ in Bulgwang, South Korea (Kim et al., 2017a), which exceeded the National Ambient Air Quality Standards (NAAQS) for the 24-h $PM_{2.5}$ level, i.e., 35 $\mu g \cdot m^{-3}$. Particularly, high (>35 $\mu g \cdot m^{-3}$) $PM_{2.5}$ concentrations at the surface began on February 19 due to weak ventilation caused by a high-pressure system that developed over China (Kim et al., 2016; Wang et al., 2018). After several days of stagnation over the Yellow Sea, the high-pressure system slowly moved eastward and passed through South Korea (Fig. S1). The high concentrations persisted in China and South Korea for more than 1 week due to the stagnant high-pressure system (Wang et al., 2018; Kim et al., 2016). High $PM_{2.5}$ concentrations lasted until February 27, with a daily average of 100 $\mu g \cdot m^{-3}$ or higher observed at most stations in South Korea (Fig. S2).

The $PM_{2.5}$ concentration over South Korea was affected by the complex combined impact of the inflow of air pollutants from China and emissions from South Korea during this episode (Kim et al., 2017a; Park et al., 2018; Seo et al., 2017). The $PM_{2.5}$ self-contributions of downwind area emissions at each supersite were Baengnyeong (BN) 0%, Bulgwang (BG) 38%, Daejeon (DJ) 44%, Honam (HN) 37%, Youngnam (YN) 56%, and Jeju (JJ) 26% during the study period, as shown in Fig. S2. The BN station in Fig. 1 is on the $PM_{2.5}$ inflow pathway from China with negligible local emissions. It experienced a rapid increase (48 $\mu g \cdot m^{-3}$) in its daily $PM_{2.5}$ concentration from 64 $\mu g \cdot m^{-3}$ on February 22–112 $\mu g \cdot m^{-3}$ on February 23 (Kim et al., 2021b; Lee et al., 2015). In this study, we selected Shandong-Hebei (SH), China, as the upwind area and the Seoul Metropolitan Area (SMA), South Korea, as the downwind area, where the aerosol optical depth (AOD), a proxy for $PM_{2.5}$, was high during the study period (Fig. S1).

2.2. Air quality simulation

We performed a series of air quality simulations using the Community Multi-scale Air Quality (CMAQ) version 4.7.1 (Byun and Schere, 2006). Meteorological input data for CMAQ were prepared using outputs from the Unified Model (UM) version 7.9, and processed with the Meteorology–Chemistry Interface Processor (MCIP) version 2.0 from the National Institute of Meteorological Science (Davies et al., 2005; Kim et al., 2017a). Tables S1 and S2 provide detailed structural information

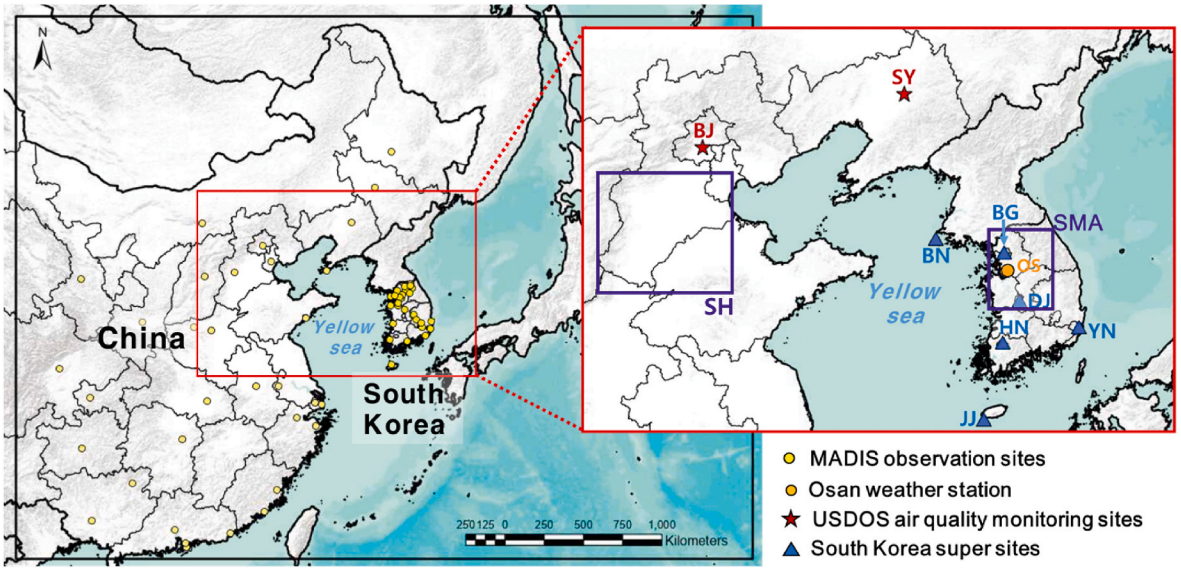

Fig. 1. The modeling domain, study areas, and observational sites used for this study. Blue boxes denote the upwind (Shandong-Hebei; SH) and downwind (Seoul Metropolitan Area; SMA) study areas. Yellow circles represent Meteorological Assimilation Data Ingest System (MADIS) observation sites. The orange circle represents Osan weather station. Red stars represent the U.S. Department of State (USDOS) air quality monitoring sites at Beijing (BJ) and Shenyang (SY). Blue triangles represent locations of South Korean supersites at Baengnyeong (BN), Bulgwang (BG), Daejeon (DJ), Honam (HN), Youngnam (YN), and Jeju (JJ). (For interpretation of the references to colour in this figure legend, the reader is referred to the Web version of this article.)

about the horizontal grid and the vertical layer, respectively. There were 9 layers below 2 km. The modeled concentrations at the first layer (0–30 m) considered as surface concentrations. Also, we conducted an aloft transport analysis on the 8th modeling layer (at a height of approximately 1200–1600 m) because lower modeling layers (i.e., the 7th modeling layer and below) were within the PBL so that they were susceptible to surface influences such as local emissions. In addition, our simulation showed that there were relatively lower $PM_{2.5}$ concentrations in the 9th or higher modeling layers compared to those in the 8th layer, which showed that the 8th modeling layer is the major pathway of aloft $PM_{2.5}$ transport.

The anthropogenic emissions inventories included the Clean Air Policy Support System (CAPSS) 2010 for South Korea and the Model Inter-Comparison Study for Asia (MICS-Asia) 2010 for the rest of Northeast Asia, including China (Li et al., 2017b). Anthropogenic emission inputs for CMAQ were prepared using the Sparse Matrix Operator Kernel Emission (SMOKE; Benjey et al., 2001) model version 2.1 to account for the spatiotemporal allocation and chemical speciation. The biogenic emissions were estimated using the Model of Emissions of Gases and Aerosols from Nature (MEGAN; Guenther et al., 2006) version 2.0. Kim et al. (2017a) has reported on the meteorological, emissions, and air quality models in extensive detail.

The simulated temperatures and wind speeds were in good agreement with observed surface data from the NCEP Meteorological Assimilation Data Ingest System (MADIS), as shown in Fig. S3. The Pearson correlation coefficients (R) of surface temperatures were 0.98 and 0.97 for China and South Korea, respectively. The R values of surface wind speeds were 0.80 and 0.68 for China and South Korea, respectively. The simulated temperatures and wind speeds at 850 hPa were also in good agreement with observed values at Osan weather station in South Korea (Fig. 1 and Fig. S4). The R values were 0.96 and 0.83 for temperatures and wind speeds, respectively. Our model performance for $PM_{2.5}$ met the statistical benchmarks suggested by Emery et al. (2017) at two U.S. Department of State (USDOS) air quality monitoring stations in China (one at the U.S. embassy in Beijing and the other at the consulate in Shenyang) and six air monitoring stations (Baengnyeong, Bulgwang, Daejeon, Honam, Youngnam, and Jeju) in South Korea (Fig. 1 and Table S3). Furthermore, the spatial distribution of simulated AOD was similar to that of observed AOD from Moderate Resolution Imaging Spectroradiometer (MODIS) during the study period (Fig. S5).

2.3. Estimation of long-range transport pathways

In this study, we applied the brute force method (BFM) that is an analytical technique used to estimate the sensitivity of the concentrations to emissions changes (Burr and Zhang, 2011; Koo et al., 2007; Thunis et al., 2019). The sensitivity is calculated from the difference between simulated $PM_{2.5}$ concentrations with/without emission perturbations. By extrapolating the sensitivity result of BFM with less than 100% emission reductions (e.g., 50%) to a 100% emission reduction, zero-out contribution (ZOC) can be estimated. In general, a 100% emission reduction for BFM is not recommended to derive ZOC due to the non-linear chemistry in the study region (Bae et al., 2022). We calculated the ZOC of upwind area emissions to downwind $PM_{2.5}$ concentrations in this study as follows:

$$ZOC = (C_{Base} - C_{Sens_E}) / \Delta E, \quad (1)$$

where, ΔE is the emissions perturbation rate (0.5 in this study, as this value has been used in many previous studies (Bae et al., 2022; Kim et al., 2021a, b; Park et al., 2021)). C_{Sens_E} is the $PM_{2.5}$ concentration simulated with a 50% reduction in all primary and precursor emissions in the upwind area. Kim et al. (2017a, b) reported that estimated ZOCs can differ by up to 10% when using an emissions perturbation rate of 50% compared with that of 100%.

A previous study reported that the contribution of the upwind to the downwind area increased from February 23 (Kim et al., 2017a); however, emissions in the upwind area were perturbed from 2 days prior (February 21–23), due to the transport time of the air pollutants. Transport pathway is critical for our analysis that relies on the ZOC. Therefore, to identify the inflow pathways for the downwind area and estimate the upwind area, back trajectory analysis was conducted using the HYSPLIT model. We selected the SMA, a downwind area, as the origin of the back trajectories. We chose altitudes of 100 and 1000 m as the analysis heights to represent the surface and aloft areas, respectively.

2.4. Analysis of impact of vertical mixing on long-range transport

The impact of vertical mixing on long-range transport was examined using Process Analysis (PA) implemented in CMAQ, which can quantify physical contributions, such as of emissions, advection, diffusion, and deposition, and chemical contributions, such as of aerosols, chemistry, and clouds, to the changes in the simulated concentrations (Gao et al., 2020; Gipson and Young, 1999; Huang et al., 2021; Liu et al., 2010).

First, the individual contributions of the three main physical processes (HADV, ZADV, and VDIF) to the $PM_{2.5}$ concentrations in the upwind and downwind areas were examined using PA (Base in Table S4). Next, the role of vertical mixing in distributing $PM_{2.5}$ concentrations was quantitatively analyzed for ZADV and VDIF. Although ZADV and VDIF affect vertical mixing of air pollutants simultaneously in the real world, a sensitivity simulation was performed by minimizing the ZADV and VDIF processes in the upwind and downwind areas to understand their individual roles in long-range air pollutant transport. The detailed information is provided in Figs. S6 and S7.

For the ZADV, the updraft (ZADV(+)) moves air pollutants from the surface to aloft, while the downdraft (ZADV(−)) moves air pollutants from a high altitude to the surface. In this study, we hypothesized that the ZADV(+) is important in the upwind area while ZADV(−) is important in the downwind area during the long-range transport of air pollutants. Therefore, we designed a set of sensitivity experiments, as shown in Fig. 2 and Table S4. The sensitivity runs were labeled as A_{up1} and D_1 (Fig. 2) and used to separately examine the impacts of ZADV(+) and VDIF in the upwind area on the $PM_{2.5}$ concentrations in the downwind area. Similarly, the A_{down2} and D_2 sensitivity simulations were used to examine the impacts of ZADV(−) and VDIF in the downwind area. Considering that ZADV and VDIF simultaneously affect the $PM_{2.5}$ concentrations in the atmosphere, additional sensitivity simulations (i.e., $A_{up1}D_1$ and $A_{down2}D_2$, which simultaneously minimized the VDIF and ZADV in upwind and downwind areas) were conducted and analyzed.

3. Results

3.1. Surface and aloft long-range transport

Back trajectories from the downwind area during the high $PM_{2.5}$ episode indicates that the speed of air mass movement was low at the surface (Fig. S3), possibly owing to the stagnant high-pressure system (Kim et al., 2017a). The wind speed was found to be ~1.5 $m \cdot s^{-1}$. In contrast, the aloft air mass was transported long-range to the downwind area through an upwind area, such as SH (Fig. 1), the Yellow Sea, and west of North Korea. Kim et al. (2017b) also reported that the AOD was high over these regions and South Korea due to movement of the air pollutants through these regions.

In the downwind area, the contributions of SH emissions to surface $PM_{2.5}$ concentrations in the SMA were 0.7, 2.9, and 6.7 $\mu g \cdot m^{-3}$, while those to aloft concentrations were 5.7, 6.5, and 4.0 $\mu g \cdot m^{-3}$ on February 23, 24, and 25, respectively (Fig. 3). The contribution of SH emissions to aloft concentration was higher than that to the surface on February 23, while the pattern of relative contribution magnitudes was reversed on February 25. The contribution of a transport pathway was examined vertically to understand its variability at different altitudes (Fig. S8). The

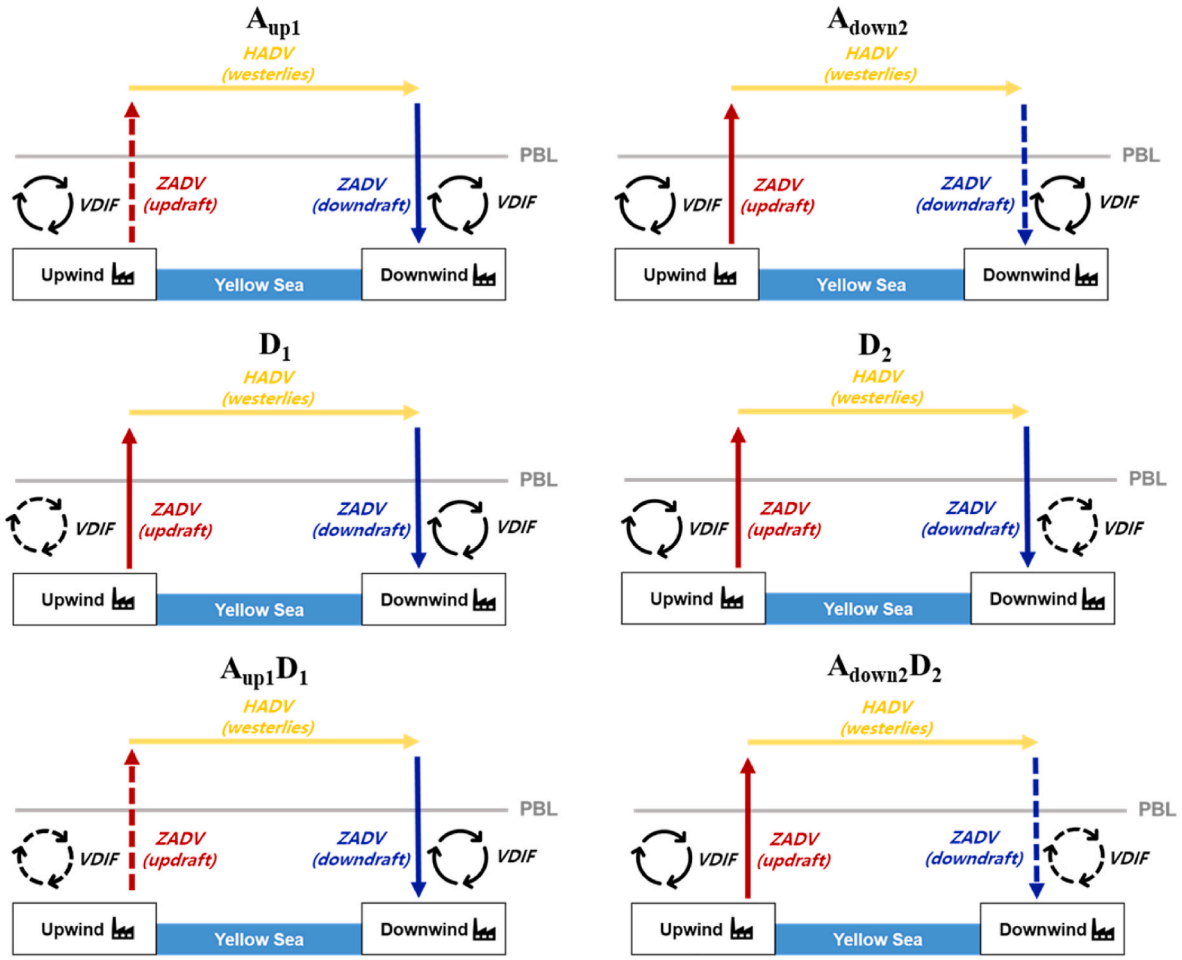

Fig. 2. Schematic diagram of the experiment designs (Table S4) that control vertical advection and diffusion over the upwind and downwind areas. The lowercase "up" and "down" indicates updraft and downdraft of vertical advection, respectively. The dotted line indicates the controlled factor.

transport pathway ("A"–"F" in Fig. 4b) was selected by referring to the back trajectory (Fig. 4a) on February 23 when the contribution of upwind area emissions was first observed in the downwind area. On February 22 (Fig. 5), the contribution of upwind area emissions on the $PM_{2.5}$ concentrations occurred horizontally from A (i.e., Beijing) to the mid-point of B and C. Particularly, the $PM_{2.5}$ contributions from the surface to an altitude of 1000 m at A (i.e., the upwind area) were $\geq$50 $\mu g \cdot m^{-3}$. The contribution was higher at an altitude of 1000–2000 m than at the surface through B and C. On February 24, the contribution was $\geq$10 $\mu g \cdot m^{-3}$ at an altitude of 1000–1500 m between C and D—which was ~500 km from the upwind area—with a $PM_{2.5}$ "tongue" often used to depict the shape of aloft high ozone in previous studies (e.g., Trickl et al., 2011; Zhang et al., 2022), which appeared from the upwind area. Particularly between C and D, the contribution of emissions from the upwind area was much more pronounced to aloft than that the surface concentrations, indicating that $PM_{2.5}$ was transported from the upwind area to C and D aloft rather than at surface. On February 25, noticeable contributions from the upwind area were further extended to E and F aloft. The aloft $PM_{2.5}$ concentrations from C–F were gradually mixed with downdraft movement. On February 26, the upwind area contributed up to 6 $\mu g \cdot m^{-3}$ to the surface concentrations in the downwind areas between E and F.

Based on these findings, the long-range transport of air pollutants during the episode can be summarized as follows: (1) surface air pollutants became aloft in the upwind area; (2) the aloft air pollutants were horizontally transported to the downwind area at high altitudes; and (3) the aloft air pollutants were mixed with those at the surface in the downwind area. These results support the assertion of previous studies by Lee et al. (2011) and Lee et al. (2019b). The following sections present our quantitative assessment on the role of vertical mixing in long-range transport.

3.2. *Process analyses of upwind and downwind $PM_{2.5}$*

The changes in the $PM_{2.5}$ concentrations owing to major physical processes, such as HADV, ZADV, and VDIF, in the upwind and downwind areas were examined using PA with CMAQ (Fig. 6). Horizontal diffusion was not analyzed because its impact on the $PM_{2.5}$ concentrations was negligible as compared to HADV (Seaman et al., 2000). Fig. 6 shows the changes in the $PM_{2.5}$ concentrations due to each process in the upwind and downwind areas. A positive value (red) in the HADV process indicated that $PM_{2.5}$ inflow by horizontal transport was higher than the outflow and the net effect was that of increased $PM_{2.5}$ concentrations in the area. In an upwind area, the HADV showed a positive value at the surface and a negative value while aloft between February 22 and 24, wherein high $PM_{2.5}$ concentrations were observed and simulated. It presented that the concentrations increased owing to HADV at the surface, but decreased at aloft altitudes of 1000–2000 m in the upwind area. In contrast, the surface $PM_{2.5}$ concentrations in a downwind area decreased by HADV between February 23 and 26 while the aloft concentrations increased.

The diurnal changes in the $PM_{2.5}$ concentrations by VDIF showed dependency on the planetary boundary layer (PBL) (Fig. 6 and S9). In both the upwind and downwind areas, the VDIF was positive near the

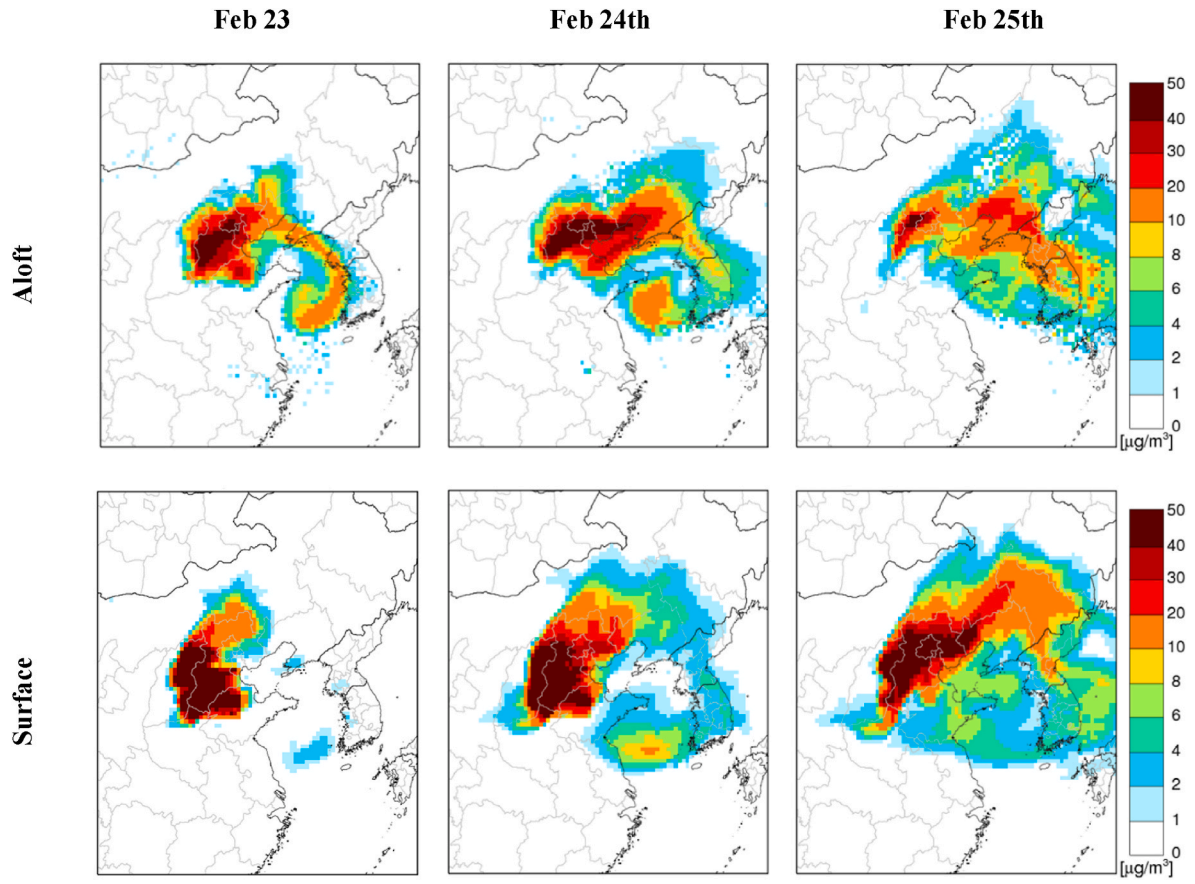

Fig. 3. Zero-out contributions of upwind area emissions to the aloft (top) and surface (bottom) $PM_{2.5}$ concentrations in Northeast Asia on February 23, (left), 24 (middle), and 25 (right), 2014. The representative heights for "aloft" and "at surface" are 1200–1600 m and 0–30 m, respectively.

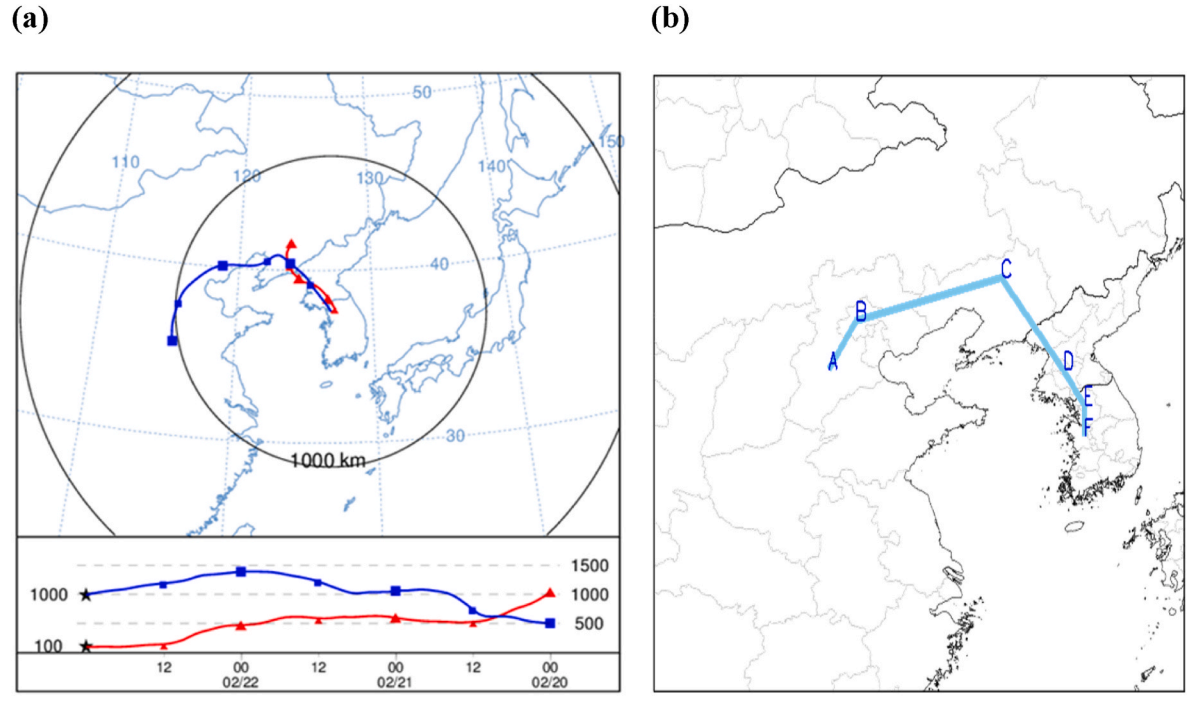

Fig. 4. Back-trajectories during the study period: (a) 72-h HYSPLIT back trajectories marked with a square or triangle at each 12-h interval released at 100 m (red line) and 1000 m (blue line) on February 23 from the downwind area. (b) Analysis path ("A"–"F") derived from the HYSPLIT back trajectories. (For interpretation of the references to colour in this figure legend, the reader is referred to the Web version of this article.)

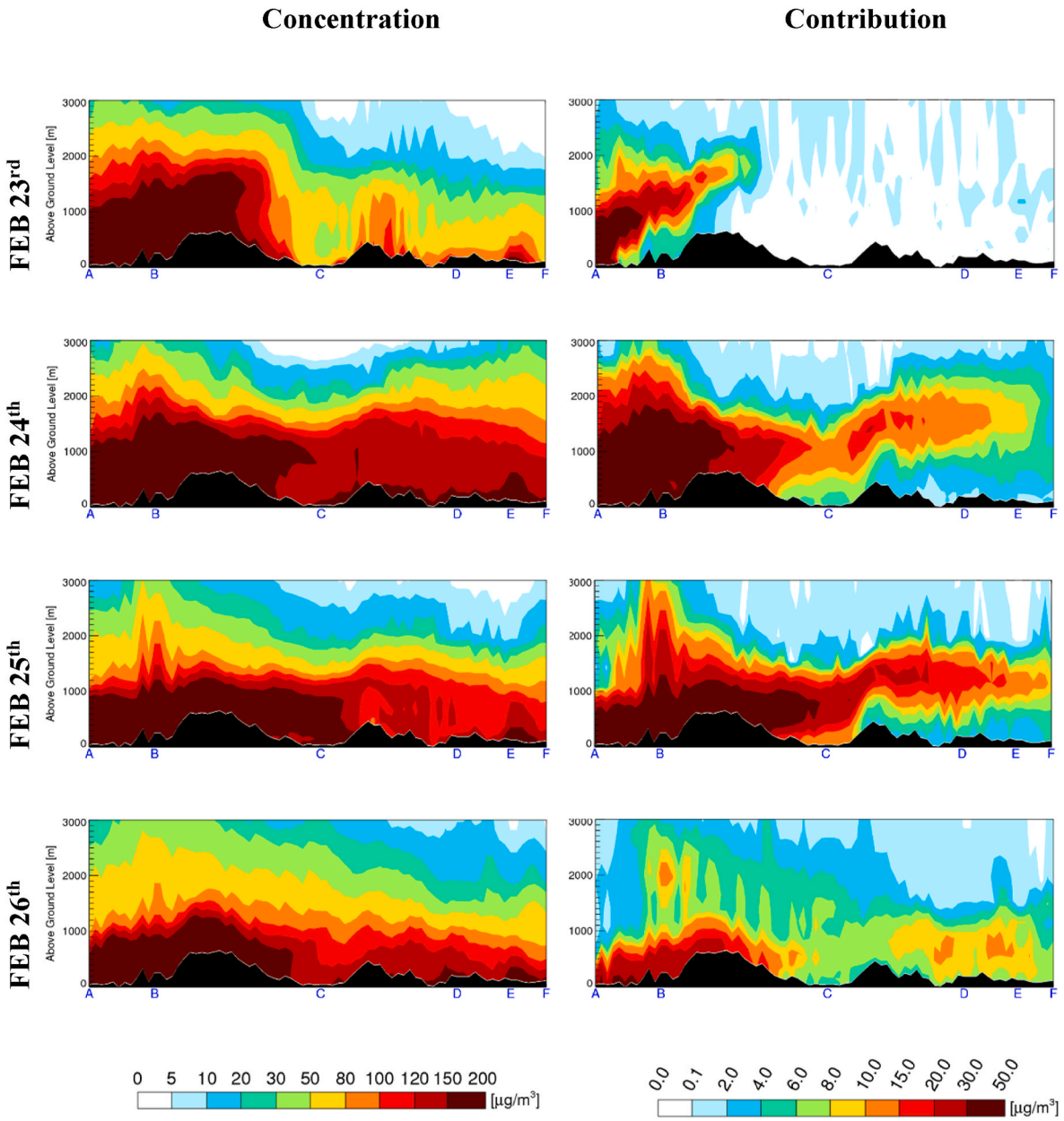

Fig. 5. Vertical distribution of the daily $PM_{2.5}$ concentrations (left) and contributions (right) of Shandong-Hebei emissions along the analysis path ("A"–"F") defined in Fig. 3(b) during February 23–26.

PBL, but negative below it (particularly at the surface) (Fig. S9). The altitude affected by the VDIF changed over time with diurnal changes of PBL throughout the study period. The ZADV and the VDIF are involved in the vertical mixing of air pollutants. However, the VDIF can mix air pollutants in both upward and downward directions depending on concentration gradients, while the ZADV determines the direction of mixing air pollutants according to the vertical wind direction. As shown in Fig. 6, during the study period, $PM_{2.5}$ moved up from a lower (negative; below 1000 m) to an upper layer (positive; above 1000 m) by the ZADV(+) in the upwind area. Similarly, in the downwind area, the $PM_{2.5}$ moved down from the upper (negative) to the lower layer (positive) by the ZADV(−) because it was dominant in South Korea during this period under the high pressure system that resulted in stagnant conditions over the Yellow Sea area when the system moved to the east of South Korea (Fig. S1).

In the upwind area, PM2.5 that was inflowed horizontally at a lower layer was moved aloft by the VDIF and ZADV and then outflowed by the HADV. In contrast, in the downwind area, $PM_{2.5}$ was inflowed by the aloft HADV and descended to the surface by the ZADV. The VDIF showed diurnal PBL-dependent changes in both the upwind and downwind areas and moved the $PM_{2.5}$ up to a height of 1500 m. The ZADV moved it up to a height of 3000 m in the upwind area and played a key role in changing its aloft concentrations to higher than that of the PBL. The VDIF only affected the change in the concentrations near the surface during nighttime when the PBL decreases, while the ZADV changed them between the surface and aloft regardless of the time during the episode. By performing a set of sensitivity simulations in which the vertical processes in the upwind and downwind areas were controlled, we demonstrated that long-range transport can be minimized by limiting vertical processes as described in Section 3.3.

3.3. *Sensitivity of vertical advection and diffusion to long-range transport*

In section 3.2, we analyzed the impact of the physical transport

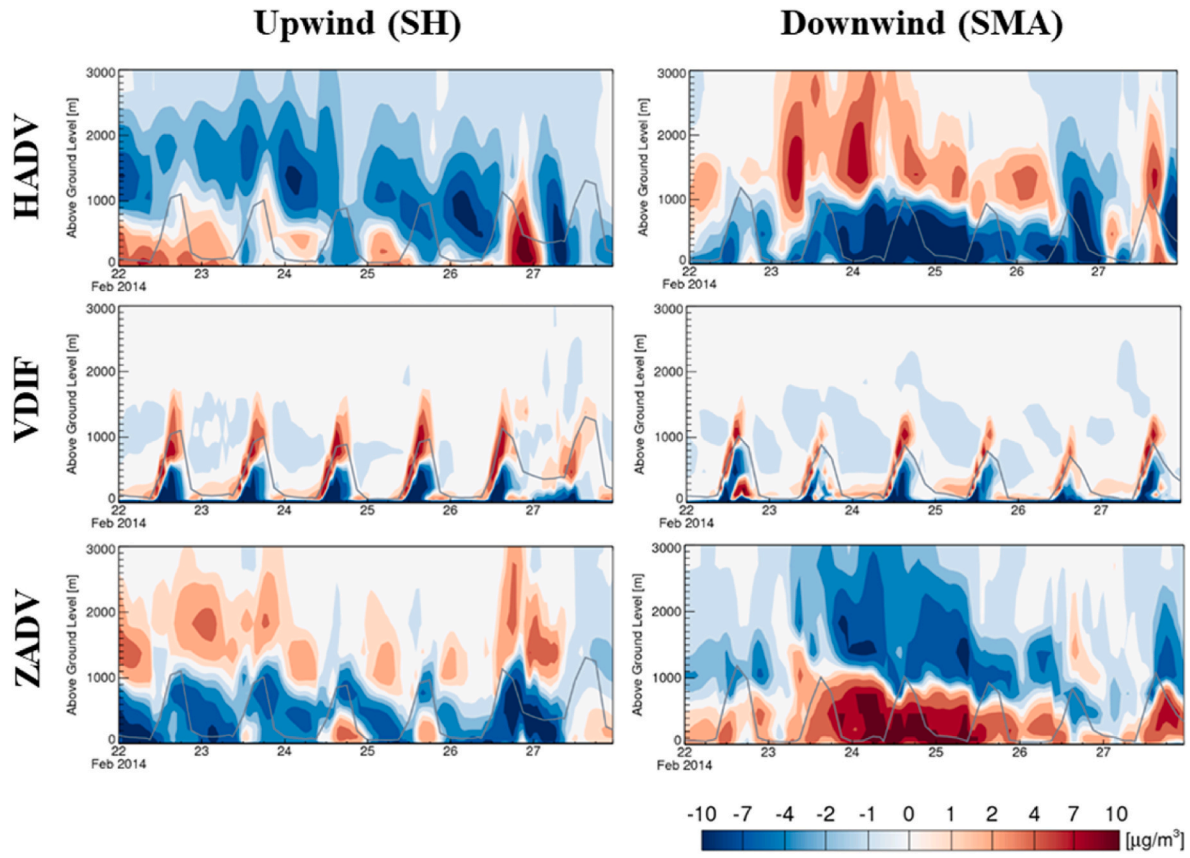

Fig. 6. Vertical distribution of $PM_{2.5}$ contributions by horizontal advection (top), vertical diffusion (middle), and vertical advection (bottom) in the upwind (left) and downwind areas (right) during the episode. The gray lines denote the planetary boundary layer heights.

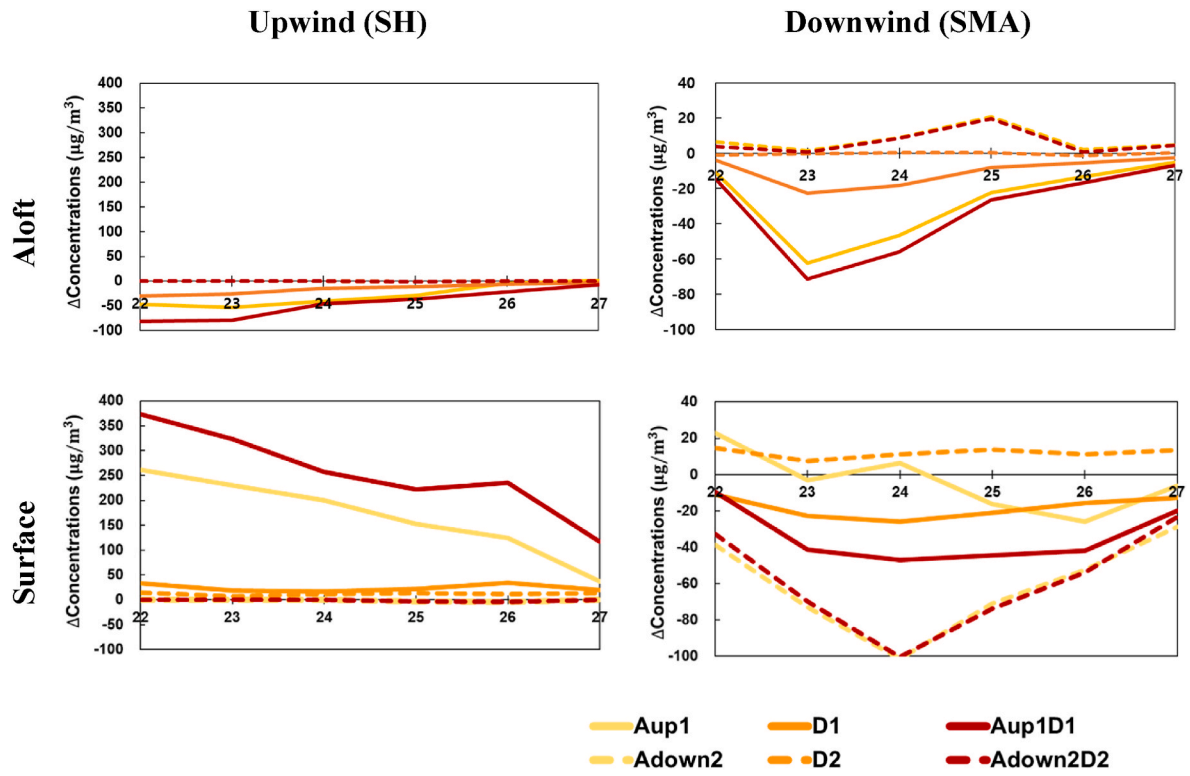

Fig. 7. Sensitivity of the aloft (top) and surface (bottom) $PM_{2.5}$ concentrations to perturbations of vertical advection over China (A_{up1}), vertical diffusion over China (D_1), simultaneous vertical advection and diffusion over China ($A_{up1}D_1$), vertical advection over South Korea (A_{down2}), vertical diffusion over South Korea (D_2), and simultaneous vertical advection and diffusion over South Korea ($A_{down2}D_2$) in the upwind (left) and downwind areas (right) during the study period.

processes, such as VDIF and ZADV, on the $PM_{2.5}$ concentrations of the upwind and downwind areas. However, it was difficult to segregate each of the upwind and downwind impacts with respect to the net impact on the downwind area. To understand the role of vertical advection and diffusion in long-range transport, we controlled each of those processes in the upwind and downwind areas, respectively and analyzed the direct impacts of those processes quantitatively through their long-range transport processes (Fig. 2 and Table S4). We focused on the impacts using maximum daily mean values because the importance of each process in long-range transport varied each date while an exceedance of the short-term (i.e., 24-h) $PM_{2.5}$ standard is determined based on the 24-h moving average of hourly $PM_{2.5}$ concentrations in South Korea. At the same time, we also present the daily mean impacts and period averaged impacts of these processes in Fig. S5 as a reference information.

When the VDIF was controlled in the upwind area (D_1), the daily averaged $PM_{2.5}$ concentrations increased up to 34 $\mu g \cdot m^{-3}$ (25%) at the surface but decreased up to 30 $\mu g \cdot m^{-3}$ (29%) aloft (layer 8; ~1200–1600 m) in the upwind area (Fig. 7). Furthermore, the daily

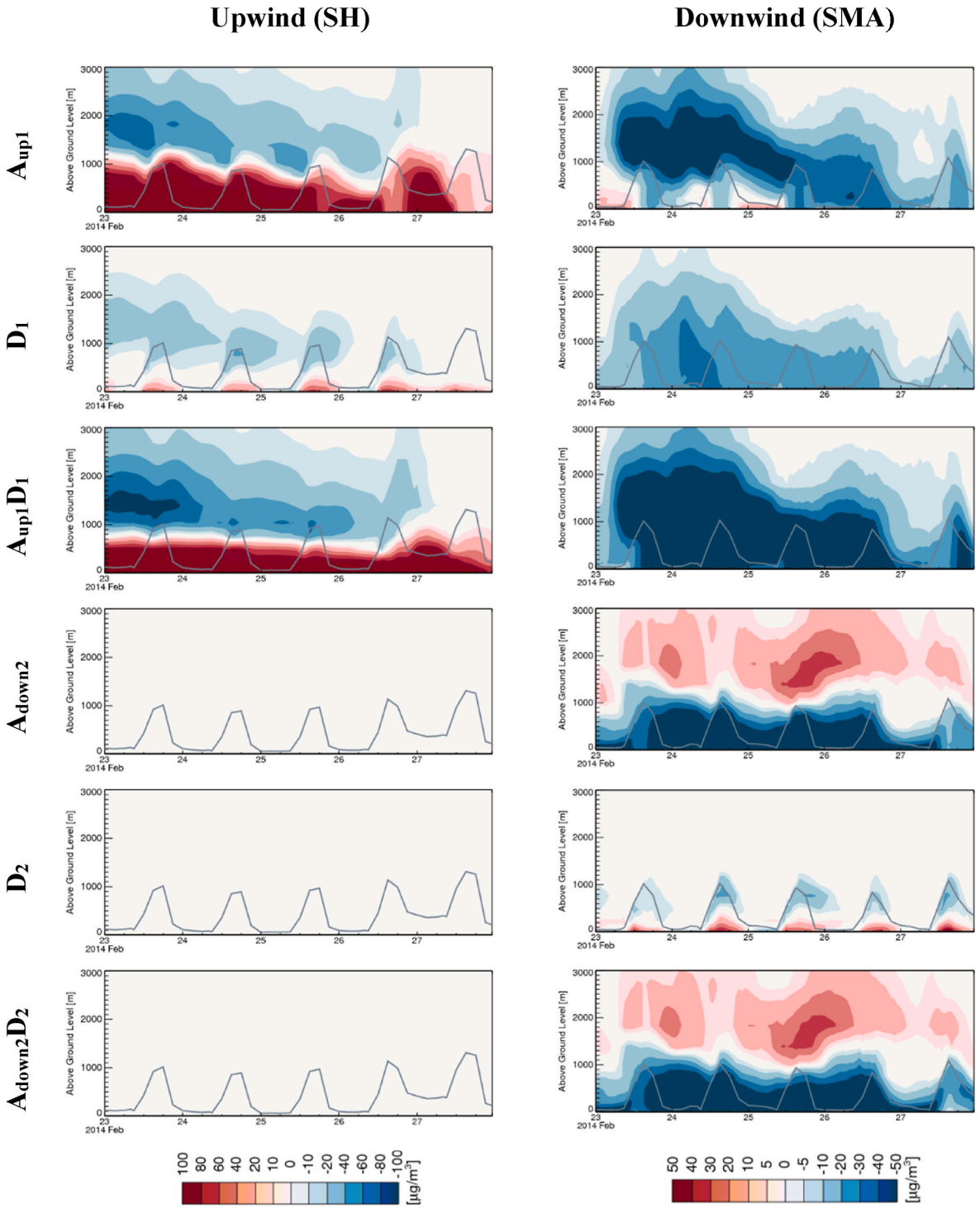

Fig. 8. Vertical distribution of upwind (left) and downwind (right) $PM_{2.5}$ sensitivity during the episode to perturbations of vertical advection over China (A_{up1}), vertical diffusion over China (D_1), simultaneous vertical advection and diffusion over China ($A_{up1}D_1$), vertical advection over South Korea (A_{down2}), vertical diffusion over South Korea (D_2), and simultaneous vertical advection and diffusion over South Korea ($A_{down2}D_2$).

averaged concentrations in the downwind area decreased up to 23 $\mu g \cdot m^{-3}$ (28%) and 26 $\mu g \cdot m^{-3}$ (15%) aloft and at the surface, respectively. As the VDIF was controlled in the upwind area, air pollutants accumulated on the surface due to minimal vertical mixing (Fig. 8). Subsequently, the $PM_{2.5}$ concentrations increased at the surface and decreased aloft in the upwind area. Moreover, the decreased aloft concentrations in the upwind area resulted in reduction of the aloft and surface concentrations in the downwind area. This indicates that the VDIF in the upwind area mixed the surface and aloft $PM_{2.5}$ and affected the long-range transport of the latter.

When the ZADV was controlled in the upwind area (A_{UP1}), the $PM_{2.5}$ concentrations increased significantly (up to 262 $\mu g \cdot m^{-3}$; 113%) at the surface during the episode and decreased aloft (up to 53 $\mu g \cdot m^{-3}$; 54%), which may be similar to the case with controlled VDIF (Fig. 7 and Table S5). However, in that case, the $PM_{2.5}$ concentrations in the upwind area only increased near the surface where the emission sources were concentrated. With controlled ZADV, the $PM_{2.5}$ concentrations increased at a height of up to 1000 m (Fig. 8) in upwind area, and the regional $PM_{2.5}$ transport from the upwind to downwind areas through the surface layers was occasionally simulated, especially when $PM_{2.5}$ concentrations in upwind area in the vicinity of downwind area increased (Fig. S10). The daily averaged aloft $PM_{2.5}$ concentrations decreased up to 62 $\mu g \cdot m^{-3}$ (73%) in the downwind area. Toward the end of the episode, the concentrations in the downwind area decreased at lower heights. The surface $PM_{2.5}$ concentrations in the downwind area decreased up to 26 $\mu g \cdot m^{-3}$ (23%) in the latter part of the episode (Fig. 7).

During the episode, the ZADV(+) in the upwind area mixed $PM_{2.5}$ up in the upwind area, similar to the VDIF, and contributed to the long-range transport of aloft air pollutants. However, the ZADV, which moved the $PM_{2.5}$ to a higher altitude than the VDIF, played a more important role in long-range transport.

When the ZADV and VDIF were simultaneously controlled in the upwind area ($A_{up1}D_1$), the daily averaged $PM_{2.5}$ concentrations at the surface in the upwind area increased up to 373 $\mu g \cdot m^{-3}$ (decreased up to 81 $\mu g \cdot m^{-3}$ aloft), which was 77 $\mu g \cdot m^{-3}$ higher than the sum of the changes in the concentrations when controlling the ZADV (262 $\mu g \cdot m^{-3}$) and VDIF (34 $\mu g \cdot m^{-3}$) at the surface (Fig. 7 and Table S5). This finding suggests that the ZADV and VDIF are mutually related and synergistic in the vertical movement of $PM_{2.5}$ from the surface to aloft. Simultaneous control in the ZADV and VDIF in an upwind area decreased the daily averaged $PM_{2.5}$ concentrations by 71 $\mu g \cdot m^{-3}$ (84%) aloft and 47 $\mu g \cdot m^{-3}$ (28%) at surface in the downwind area.

Both local emissions and long-range transport from an upwind area contributed to the $PM_{2.5}$ concentrations in a downwind area. When the VDIF was controlled in the downwind area (D_2), its decrease caused the $PM_{2.5}$ concentrations at the surface to increase up to 15 $\mu g \cdot m^{-3}$ (15%) with increased contribution of local emissions near the surface (Figs. 7 and 8). If the aloft concentrations are higher than at the surface, the VDIF can effectively increase the concentrations at the surface by vertical mixing. However, as shown in Fig. 6, there was no clear movement to the surface by the VDIF below the PBL altitude. In the D_2 simulation, the $PM_{2.5}$ concentrations in the downwind area decreased below the PBL altitude, mainly during the daytime.

When the ZADV(−) decreased (A_{down2}) in the downwind area, the daily averaged $PM_{2.5}$ concentrations increased aloft in the downwind area, but decreased at the surface (Fig. 8). Particularly, when high pressure in the Yellow Sea region affected the downwind area in the middle of the episode (February 24–25), the daily averaged $PM_{2.5}$ concentrations decreased up to 101 $\mu g \cdot m^{-3}$ (60%) at the surface and increased up to 21 $\mu g \cdot m^{-3}$ (59%) aloft (Fig. 7). In the downwind area, the ZADV(−) mixed aloft $PM_{2.5}$ down to the surface, resulting in an increase in the $PM_{2.5}$ concentrations at the surface during the episode. Aloft emissions source was absent; therefore, we can infer that the ZADV (−) in the downwind area and horizontal long-range transport played crucial roles in increasing the $PM_{2.5}$ concentrations at the surface.

The simultaneous control of the ZADV and VDIF in a downwind area decreased the daily averaged $PM_{2.5}$ concentrations up to 100 $\mu g \cdot m^{-3}$ (59%) at the surface, similar to the change in the concentrations with decreased ZADV (Table S5). This indicates that the mix-down by the ZADV played a more significant role in increasing the surface concentrations than by the VDIF. Moreover, unlike the VDIF, the ZADV(−) effectively mixed $PM_{2.5}$ down during the night as well. However, unlike the effect of the VDIF, which consistently changes with the diurnal PBL variations, the effect of the ZADV was expected to vary according to the weather conditions related to vertical wind.

Fig. 9 summarizes the findings presented in sections 3.1–3.3. During the episode, the surface $PM_{2.5}$ and its precursors in an upwind area were mixed up by the VDIF and ZADV. Subsequently, $PM_{2.5}$ was transported long-range to the downwind area as aloft and mixed down from a high altitude to the surface of downwind area by ZADV(−) under high-pressure conditions. Consequently, the surface $PM_{2.5}$ emissions in the upwind area contributed to the surface $PM_{2.5}$ concentrations in the downwind area via the transport mechanism, despite “stagnant” meteorological conditions during the high $PM_{2.5}$ episode.

4. Conclusions

In this study, we examined the role of vertical mixing in the long-range transport of $PM_{2.5}$ during the high $PM_{2.5}$ episode in late February 2014, across the Northeast Asia region. As vertical mixing is a combined physical process that consists of VDIF and ZADV, we analyzed its effect on $PM_{2.5}$ accumulation/dispersal using a chemical transport model with a tool to separately quantitate the effects of the VDIF and ZADV.

During the study period, the high-pressure system slowly moved and consequently transported $PM_{2.5}$ from an upwind to a downwind area over several days. We found that the long-range transport at high altitudes was more effective at increasing $PM_{2.5}$ concentrations in the downwind area than long-range transport at low altitudes during this $PM_{2.5}$ accumulation period at the downwind area. Our analysis showed that $PM_{2.5}$ accumulated at the surface in the upwind area became mixed with air masses up to altitudes of ~2000 m and were transported to the downwind area as aloft, where it was mixed down to the surface, resulting in large increases in surface $PM_{2.5}$ concentrations in downwind area. Throughout these processes, the daily averaged concentrations decreased up to 373 $\mu g \cdot m^{-3}$ by the upward ZADV and VDIF at and near the surface in the upwind area. The synergistic relationship between them contributed to the vertical mixing of $PM_{2.5}$ in the upwind area. In contrast, the daily averaged surface $PM_{2.5}$ concentration in the downwind area increased up to 100 $\mu g \cdot m^{-3}$ by the downward ZADV and VDIF. We note that the downward ZADV over the downwind area was the major contributor to the increase in the surface $PM_{2.5}$ concentrations, as compared to the VDIF, because the ZADV brought $PM_{2.5}$ inflow occurring at altitudes higher than the mixing heights over the downwind area to the surface. This mechanism became more dominant during the nighttime because the intensity of the VDIF is smaller during the nighttime than during the daytime.

Our results demonstrated the significant role of vertical mixing in regional long-range transport of $PM_{2.5}$ in Northeast Asia. As air pollutants can be horizontally transported above the PBL from upwind to downwind areas, surface observations may not be reliably sufficient to explain the increased $PM_{2.5}$ in the downwind area. Therefore, further in-depth model analysis with three-dimensional observations, including surface, aircraft, and satellite measurements, is warranted. Additionally, the horizontal and vertical characteristics of $PM_{2.5}$ transport can vary depending on weather conditions. As climate changes also affect the weather conditions in the long term, its related pattern of long-range transport should be analyzed in future studies.

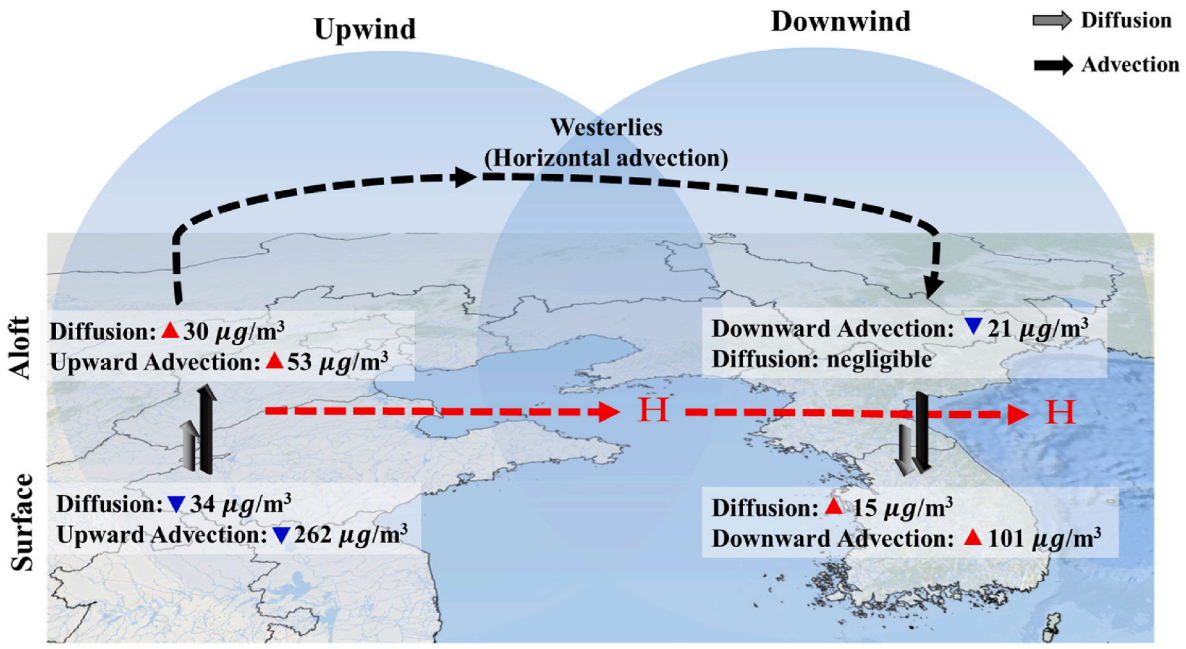

Fig. 9. Quantified maximum impacts of vertical advection and diffusion on the long-range transport of $PM_{2.5}$ in the upwind and downwind areas during the episode.

Author statement

Eunhye Kim: Conceptualization, Investigation, Visualization, Writing- Original draft. Byeong-Uk Kim: Conceptualization, Writing-Reviewing & Editing. Yoon-Hee Kang: Investigation, Writing- Original draft. Hyun Cheol Kim: Software, Writing- Reviewing & Editing. Soontae Kim: Conceptualization, Writing- Original draft, Supervision.

Declaration of competing interest

The authors declare that they have no known competing financial interests or personal relationships that could have appeared to influence the work reported in this paper.

Data availability

Data will be made available on request.

Acknowledgment

This work was supported by the National Air Emission Inventory and Research Center (NAIR); and Samsung Advanced Institute of Technology. HCK was partially supported by NOAA grant NA19NES4320002. The scientific results and conclusions, as well as any views or opinions expressed herein, are those of the author(s) and do not necessarily reflect the views of NOAA or the Department of Commerce. The authors thanks the National Institute of Meteorological Sciences (NIMS), South Korea, for providing meteorological data. The authors also thanks the National Institute of Environmental Research (NIER), South Korea, for providing surface air quality observation data.

Appendix A. Supplementary data

Supplementary data to this article can be found online at https://doi.org/10.1016/j.envpol.2022.120997.

References

Benjey, W., et al., 2001. Implementation of the SMOKE Emission Data Processor and SMOKE Tool Input Data Processor in Models-3. US EPA.
Burr, M.J., Zhang, Y., 2011. Source apportionment of fine particulate matter over the Eastern US Part I: source sensitivity simulations using CMAQ with the Brute Force method. Atmos. Pollut. Res. 2 (3), 300–317.
Byun, D.W., Schere, K.L., 2006. Review of the governing equations, computational algorithms, and other components of the Models-3 Community Multiscale Air Quality (CMAQ) modeling system. Appl. Mech. Rev. 59 (2), 51–77.
Bae, M., et al., 2022. An observation-based adjustment method of regional contribution estimation from upwind emissions to downwind PM2.5 concentrations. Environ. Int. 163, 107214.
Bae, C., et al., 2019. Long-range transport influence on key chemical components of PM2.5 in the Seoul metropolitan area, South Korea, during the years 2012–2016. Atmosphere 11, 48.
Chen, D., et al., 2021. Impact of inter-annual meteorological variation from 2001 to 2015 on the contribution of regional transport to PM2. 5 in Beijing, China. Atmos. Environ. 260, 118545.
Chen, T.F., et al., 2014. Modeling direct and indirect effect of long-range transport on atmospheric PM2. 5 levels. Atmos. Environ. 89, 1–9.
Choi, J., et al., 2019. Impacts of local vs. trans-boundary emissions from different sectors on PM2.5 exposure in South Korea during the KORUS-AQ campaign. Atmos. Environ. 203, 196–205.
Chuang, M.-T., et al., 2008. Simulation of long-range transport aerosols from the Asian continent to Taiwan by a southward Asian high-pressure system. Sci. Total Environ. 406, 168–179.
Davies, T., et al., 2005. A new dynamical core for the Met Office's global and regional modelling of the atmosphere. Q. J. R. Meteorol. Soc. 131 (608), 1759–1782.
Emery, C., et al., 2017. Recommendations on statistics and benchmarks to assess photochemical model performance. J. Air Waste Manage. Assoc. 67 (5), 582–598.
Gao, Y., et al., 2020. Characteristics and sources of PM2. 5 with focus on two severe pollution events in a coastal city of Qingdao, China. Chemosphere 247, 125861.
Ge, B., et al., 2018. Air pollution over the North China Plain and its implication of regional transport: a new sight from the observed evidences. Environ. Pollut. 234, 29–38.
Gipson, G.L., Young, J., 1999. Science Algorithms of the EPA Models-3 Community Multiscale Air Quality (CMAQ) Modeling System. Process analysis. US EPA.
Guenther, A., et al., 2006. Estimates of global terrestrial isoprene emissions using MEGAN (model of emissions of Gases and aerosols from nature). Atmos. Chem. Phys. 6 (11), 3181–3210.
Huang, C., et al., 2021. Study on the variation of air pollutant concentration and its formation mechanism during the COVID-19 period in Wuhan. Atmos. Environ. 251, 118276.
Itahashi, S., et al., 2017. Nitrate transboundary heavy pollution over East Asia in winter. Atmos. Chem. Phys. 17, 3823–3843.
Kim, B.-U., et al., 2017a. Spatially and chemically resolved source apportionment analysis: case study of high particulate matter event. Atmos. Environ. 162, 55–70.
Kim, E., et al., 2021a. Sensitivity of fine particulate matter concentrations in South Korea to regional ammonia emissions in Northeast Asia. Environ. Pollut. 273, 116428.
Kim, E., et al., 2021b. Direct and cross impacts of upwind emission controls on downwind PM2.5 under various ammonia conditions. Environ. Pollut. 115794.
Kim, H.C., et al., 2017b. Regional contributions to particulate matter concentration in the Seoul metropolitan area, South Korea: seasonal variation and sensitivity to meteorology and emissions inventory. Atmos. Chem. Phys. 17, 10315–10332.

Kim, H.C., et al., 2016. Synoptic perspectives on pollutant transport patterns observed by satellites over East Asia: case studies with a conceptual model. Atmos. Chem. Phys. Discuss. 1–30.
Koo, B., et al., 2007. Implementing the decoupled direct method for sensitivity analysis in a particulate matter air quality model. Environ. Sci. Technol. 41 (8), 2847–2854.
Lee, S., et al., 2011. High-PM10 concentration episodes in Seoul, Korea: background sources and related meteorological conditions. Atmos. Environ. 45 (39), 7240–7247.
Lee, T., et al., 2015. Characterization of aerosol composition, concentrations, and sources at Baengnyeong Island, Korea using an aerosol mass spectrometer. Atmos. Environ. 120, 297–306.
Lee, S., et al., 2019a. Analysis of long-range transboundary transport (LRTT) effect on Korean aerosol pollution during the KORUS-AQ campaign. Atmos. Environ. 204, 53–67.
Lee, H.J., et al., 2019b. Impacts of atmospheric vertical structures on transboundary aerosol transport from China to South Korea. Sci. Rep. 9, 1–9.
Lei, L., et al., 2021. Vertical distributions of primary and secondary aerosols in urban boundary layer: insights into sources, chemistry, and interaction with meteorology. Environ. Sci. Technol. 55 (8), 4542–4552.
Li, D., et al., 2017a. Identification of long-range transport pathways and potential sources of PM2. 5 and PM10 in Beijing from 2014 to 2015. J. Environ. Sci. 56, 214–229.
Li, M., et al., 2017b. MIX: a mosaic Asian anthropogenic emission inventory under the international collaboration framework of the MICS-Asia and HTAP. Atmos. Chem. Phys. 17 (2), 935–963.
Liu, X.-H., et al., 2010. Understanding of regional air pollution over China using CMAQ, part II. Process analysis and sensitivity of ozone and particulate matter to precursor emissions. Atmos. Environ. 44, 3719–3727.
Park, E.H., et al., 2018. Characteristics of PM2.5 and its chemical constituents in beijing, Seoul, and nagasaki. Air Qual. Atmos. Health 11 (10), 1167–1178.
Park, J., et al., 2021. Contributions of ammonia to high concentrations of PM2. 5 in an urban area. Atmosphere 12 (12), 1676.
Liu, Y., et al., 2021. Impact of residual layer transport on air pollution in Beijing, China. Environ. Pollut. 271, 116325.
Park, J.S., et al., 2009. Characteristic large-scale circulation anomalies associated with persistent features of extreme precipitation over northeast Asia from premonsoon season to monsoon season. J. Geophys. Res. Atmos. 114 (D11).
Pei, L., et al., 2018. Increasing persistent haze in Beijing: potential impacts of weakening East Asian winter monsoon is associated with northwestern Pacific sea surface temperature trends. Atmos. Chem. Phys. 18, 3173–3183.
Reis, S., et al., 2012. From acid rain to climate change. Science 338, 1153–1154.
Seaman, N.L., et al., 2000. Meteorological modeling for air-quality assessments. Atmos. Environ. 34, 2231–2259.
Seinfeld, J.H., Pandis, S.N., 2006. Atmos. Chem. Phys.: from Air Pollution to Climate Change, second ed. John Wiley and Sons, New York.
Seo, J., et al., 2017. On the multiday haze in the Asian continental outflow: the important role of synoptic conditions combined with regional and local sources. Atmos. Chem. Phys. 17 (15), 9311–9332.
Sharan, M., Yadav, A.K., Singh, M.P., Agarwal, P., Nigam, S., 1996. A mathematical model for the dispersion of air pollutants in low wind conditions. Atmos. Environ. 30 (8), 1209–1220.
Shen, L., et al., 2022. Regional transport patterns for heavy PM2. 5 pollution driven by strong cold airflows in Twain-Hu Basin, Central China. Atmos. Environ. 269, 118847.
Shimadera, H., et al., 2016. Evaluation of air quality model performance for simulating long-range transport and local pollution of PM 2.5 in Japan. Adv. Meteorol. 1–13, 2016.
Shin, H.J., et al., 2016. Chemical Characteristics of High PM Episodes Occurring in Spring 2014, Seoul, Korea. Adv. Meteorol., 2424875
Thunis, P., et al., 2019. Source apportionment to support air quality planning: strengths and weaknesses of existing approaches. Environ. Int. 130, 104825.
Trickl, T., et al., 2011. High-ozone layers in the middle and upper troposphere above Central Europe: potential import from the stratosphere along the subtropical jet stream. Atmos. Chem. Phys. 11 (17), 9343–9366.
Uno, I., et al., 2020. Paradigm shift in aerosol chemical composition over regions downwind of China. Sci. Rep. 10 (1), 1–11.
Wang, J., et al., 2016. Long range transport of nitrate in the low atmosphere over Northeast Asia. Atmos. Environ. 144, 315–324.
Wang, X., et al., 2018. Characteristics and classification of PM2.5 pollution episodes in Beijing from 2013 to 2015. Sci. Total Environ. 170–179.
Xiao, Z., et al., 2020. Impacts of regional transport and boundary layer structure on the PM2.5 pollution in Wuhan, Central China, Atmos. Environ. Times 230, 117508.
Yan, Y., et al., 2022. Synoptic condition and boundary layer structure regulate PM2.5 pollution in the Huaihe River Basin, China. Atmos. Res. 269, 106041.
You, S., et al., 2021. The role of a distant typhoon in extending a high PM2.5 episode over Northeast Asia. Atmos. Environ. 118480.
Zhang, Y., et al., 2022. Influences of stratospheric intrusions to high summer surface ozone over a heavily industrialized region in northern China. Environ. Res. Lett. 17 (9), 094023.